Spin Crossover in a Catenane Supramolecular System

José Antonio Real,* Enrique Andrés, M. Carmen Muñoz,
Miguel Julve, Thierry Granier, Azzedine Bousseksou,
François Varret

The compound [Fe(tvp)$_2$(NCS)$_2$] · CH$_3$OH, where tvp is 1,2-di-(4-pyridyl)-ethylene, has been synthesized and characterized by x-ray single-crystal diffraction. It consists of two perpendicular, two-dimensional networks organized in parallel stacks of sheets made up of edge-shared [Fe(II)]$_4$ rhombuses. The fully interlocked networks define large square channels in the [001] direction. Variable-temperature magnetic susceptibility measurements and Mössbauer studies reveal that this compound shows low-spin to high-spin crossover behavior in the temperature range from 100 to 250 kelvin. The combined structural and magnetic characterization of this kind of compound is fundamental for the interpretation of the mechanism leading to the spin crossover, which is important in the development of electronic devices such as molecular switches.

The electronic spin crossover phenomenon is a type of molecular magnetism (*1*, *2*) that occurs in some six-coordinate, first-row transition metal complexes. It is the result of an electronic instability driven by external constraints (temperature, pressure, or electromagnetic radiation) (*3–5*), which induce structural changes at molecular and lattice levels (*6*). Six-coordinate iron(II) ($3d^6$) spin crossover compounds are among the systems studied in most detail; they change reversibly from diamagnetic ($S = 0$) to paramagnetic ($S = 2$) spin states. In the solid state, cooperative first-order spin transition (ST) takes place at a well-defined critical temperature for a few of these compounds, some of which show thermal hysteresis.

Such properties have interested many different research groups because ST compounds could be used as molecular switches in new electronic devices because of their bistable nature (*7–10*). Light-induced excited spin state trapping (LIESST) (*11*) and ligand-driven light-induced spin changes (LD-LISC) are two examples of how quantitative $^1A_1(S = 0) \Leftrightarrow {}^5T_2$ $(S = 2)$ reversible transformation may be achieved. In the former case, the sample is irradiated with green light (550 nm) at low temperature (<50 K) to induce the $^1A_1 \rightarrow {}^1T_1$ absorption band transition, whereas in the latter case, photochemical cis–trans isomerization of the ligand occurs (*12*, *13*). A display based on an iron(II) complex has been recently reported (*14*), which takes advantage of the dramatic change of color and the large thermal hysteresis accompanying the ST.

We have attempted to clarify the nature of the cooperative mechanism in spin crossover systems by correlating the structural changes with magnetic susceptibility, Mössbauer spectroscopy, and calorimetry data (*15–17*). The aim is to define the main factors that control abruptness, hysteresis, and critical temperature to design new materials that might be used in molecular devices. To date, the major source of information on ST systems comes from mononuclear iron(II) compounds where, as a consequence of the spin conversion, molecular distortions spread through the whole crystal by means of intermolecular interactions.

The cooperativity in these systems could be enhanced by controlling both intra- and intermolecular interactions. Cooperativity can be achieved by using suitable bridging ligands. A series of dimeric iron(II) spin crossover compounds were prepared and investigated. The most remarkable feature of this family of compounds is the occurrence of a double-step spin transition. The two-step character is attributable to the synergistic effect between intramolecular and intermolecular interactions (*18*). A further step would consist of extending the connectivity among iron(II) ions by polymerizing a molecular fragment that could undergo spin conversion. In fact, one example of a two-dimensional (2D) spin crossover system that exhibits an abrupt spin transition has been reported (*19*); the question is whether this behavior is intrinsic to this kind of polymeric system. In this context, we report here the results concerning a polymeric spin crossover system of formula [Fe(tvp)$_2$(NCS)$_2$] · CH$_3$OH (tvp = 1,2-di-(4-pyridyl)-ethylene), which is unusual in that it is made up of interlocking 2D networks (*20*). Interlocked macrocycles of this kind are called catenanes.

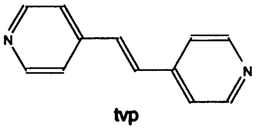

(1)

Compound 1 was synthesized (*21*) as a dark red powder by reacting methanolic solutions of iron(II)–NCS$^-$ (1:2 metal-to-ligand molar ratio) with an excess of tvp. Single crystals suitable for x-ray diffraction were isolated by slow diffusion in an H-shaped tube. All operations were carried out under an argon atmosphere.

The x-ray crystal structure of 1 (*22*)

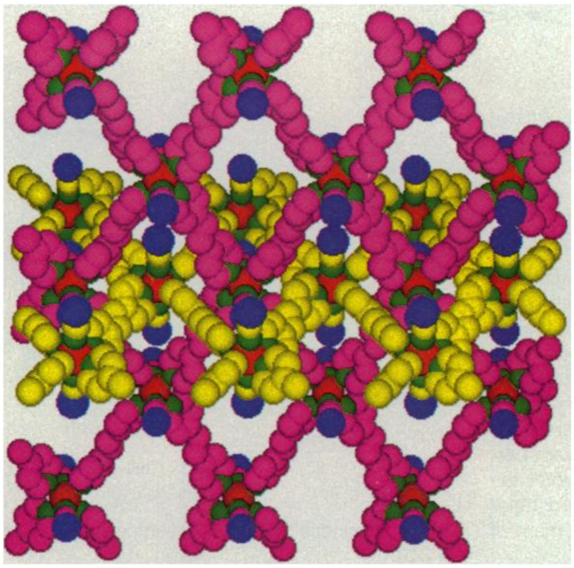

Fig. 1. Interlocking of two layers of **1** in the [001] direction. Deep red, green, and blue correspond to Fe, N, and S atoms. The C atoms of differents layers are block-colored (pink and yellow).

J. A. Real, E. Andrés, M. Julve, Departament de Química Inorgànica, Facultat de Química, Universitat de València, Dr. Moliner 50, 46100 Burjassot, València, Spain.
M. C. Muñoz, Departamento de Física Aplicada, Universidad Politécnica de València, Camino de Vera s/n, 46071 València, Spain.
T. Granier, Laboratoire de Cristallographie et de Physique Cristalline (URA 144, CNRS), Université de Bordeaux I, 33405 Talence, France.
A. Bousseksou, Laboratoire de Chimie de Coordination, 205 Route de Narbonne, 31077 Toulouse, France.
F. Varret, Laboratoire d'Optique et Magnétisme, CNRS, EPJ0035, Université de Versailles, 45 Avenue des États Unis, 78035 Versailles, France.

*To whom correspondence should be addressed.

shows the occurrence of two perpendicular, fully interlocked 2D networks (Fig. 1) constituted by parallel layers separated by 11.3 Å. The iron(II) lies in a compressed octahedron with two *trans*-thiocyanato ligands filling the axial positions and four pyridine nitrogen atoms building the basal plane [Fe(II)–N(CS) = 2.061 Å; Fe(II)–N(tvp) = 2.196 Å]. The two pyridine rings and the ethylene group of each tvp ligand are coplanar. The four pyridine units associated with each metal atom are arranged in propeller fashion (dihedral angle, 51.8°). Each tvp ligand connects two iron(II) ions defining the edges of a $[Fe(II)]_4$ rhombus: The metal-metal separation through the tvp ligand is 13.66 Å, whereas the metal-metal distances through the diagonals of the rhombus are 22.59 and 15.36 Å, respectively. Despite the strict D_{4h} symmetry of the iron(II) site, the particular disposition of the ethylene groups defines a significantly elongated rhombus (the internal angles are 111.55° and 68.44°).

The edge-shared rhombuses define the grid-layered structures mentioned above, with all of the iron(II) ions in a coplanar sheet. Parallel sheets are displaced so that the iron centers of the first sheet are vertically above those of the third, fifth, and further odd-numbered sheets, while vertically above the midpoints of $[Fe(II)]_4$ rhombuses of the even-numbered sheets (see Fig. 2). An equivalent stack of sheets is found in planes perpendicular to the first set, defining large square channels orientated in the [001] direction (see Fig. 3), where the solvent molecules are located.

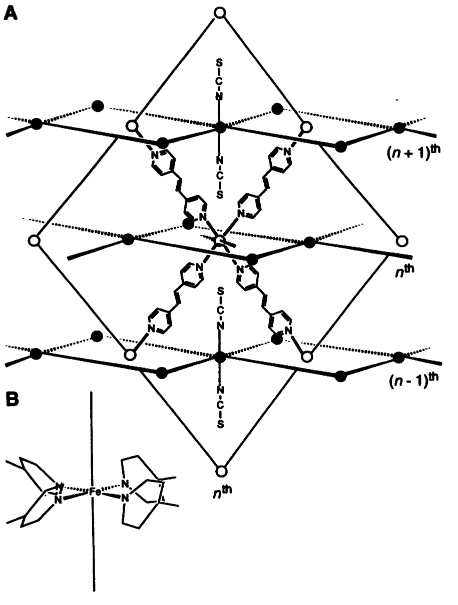

Fig. 2. (**A**) Scheme of the interpenetrating sheets orientated in the [110] direction, showing the particular disposition of the tvp ligands leading to the rhombus grid, the alternatively displaced sheets (along [001]), and the orientation of the trans NCS^- ligands along the large diagonal of the $[Fe(II)]_4$ rhombuses [black and white spheres represent iron(II) ions, which belong to different perpendicular networks; the straight line denotes the tvp ligand]. (**B**) View of the coordination octahedron, emphasizing the propeller arrangement of the four basal pyridines.

The high-spin to low-spin conversion in **1** was followed by measurement of the molar magnetic susceptibility χ_m and Mössbauer studies as a function of temperature *T*. As observed from these data, the extent and steepness of the spin conversion are very sensitive to the sample preparation and show different high- and low-spin residual fractions at low and high temperature as well as different cooperativity. The magnetic behavior of two different samples (denoted A and B) is illustrated in Fig. 4 (*23*). The χ_mT product remains practically constant from room temperature to 250 K and then decreases to reach a plateau in which residual paramagnetism is present. The χ_mT values for warming and cooling modes show that the thermal hysteresis effect, if present, is less than 0.5 K. The temperature evolution of the Mössbauer spectra (corresponding to sample A) shown in Fig. 5 agrees with the magnetic curve. The dominant doublet observed at room temperature, characterized by the quadrupole splitting $\Delta E_q = 2.108(6)$ mm s^{-1} and isomer shift IS = 1.00(3) mm s^{-1} (numbers in parentheses are standard errors in the last digit), corresponds to the $S = 2$ high-spin ground state of iron(II). As the temperature is lowered, a doublet between the two former peaks appears; its intensity increases at the expense of the former with decreasing temperature. Its characteristics at 5 K are $\Delta E_q = 0.193(2)$ mm s^{-1} and IS = 0.449(2) mm s^{-1}, typical of the $S = 0$ low-spin ground state of iron(II). The spin conversion is incomplete: high-spin fractions n_{hs} of 13% at 5 K and of 66% at 293 K are found in sample A.

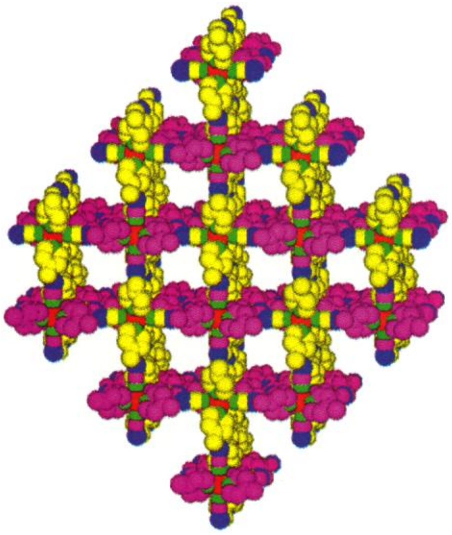

Fig. 3. Space-filling representation of the structure of **1** in the [110] direction, emphasizing the large channels formed by the interlocking of the two bidimensional nets.

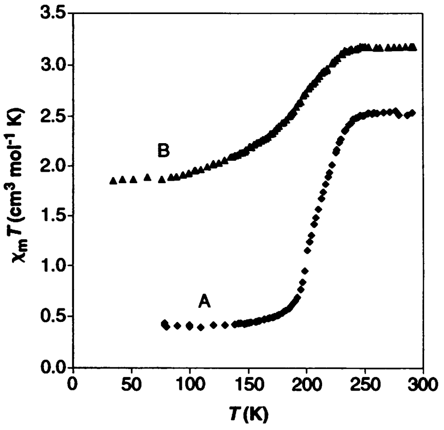

Fig. 4. Magnetic properties of samples A and B of **1** (*23*).

The presence of residual paramagnetism and diamagnetism described above is not uncommon in spin crossover systems and is generally attributed to subtle effects induced by the presence of crystalline defects and molecular inclusions (counterions or solvent molecules) or both. The synthetic procedure influences the above-mentioned factors: the magnetic properties of **1** are very sensitive to the size and quality of the

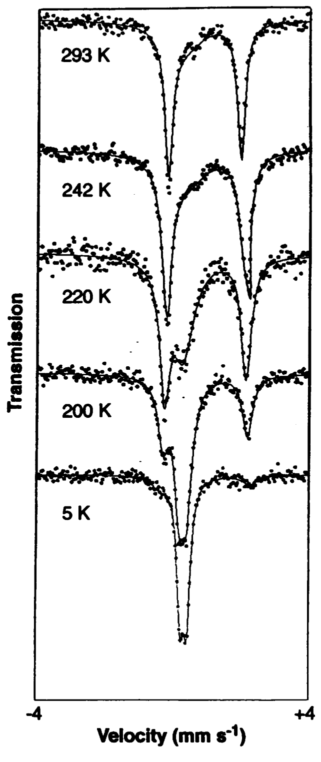

Fig. 5. A series of ^{57}Fe-Mössbauer spectra (sample A) for a representative set of temperatures (*T* = 293–5 K), displaying the $^5T_2$ (high-spin) ⇔ $^1A_1$ (low-spin) conversion.

crystals (*23*), possibly because we are dealing with a singular extended system with large channels, where the factors mentioned above are likely to exert a greater influence on spin conversion than in related molecular systems.

Catenanes are of great interest in topological stereochemistry (*24*), not only for aesthetic or intellectual pleasure but also because of their potential derived properties. Supramolecular systems have attracted the attention of many research groups because of their photochemical (*25*) and magnetic properties that can result from the interaction among their subunits. Detailed structural and magnetic characterization sheds light on the mechanisms leading to these properties, such as the cooperative mechanisms of spin crossover studied here.

REFERENCES AND NOTES

1. E. A. Boudreaux and L. N. Mulay, Eds., *Theory and Applications of Molecular Paramagnetism* (Wiley, New York, 1976).
2. O. Kahn, *Molecular Magnetism* (VCH, New York, 1993).
3. P. Gütlich, *Struct. Bonding (Berlin)* **44**, 83 (1981); P. Gütlich, A. Hauser, H. Spiering, *Angew. Chem. Int. Ed. Engl.* **33**, 2024 (1994).
4. E. König, *Struct. Bonding (Berlin)* **76**, 51 (1991).
5. P. Gütlich and A. Hauser, *Coord. Chem. Rev.* **97**, 1 (1990).
6. E. König, *Prog. Inorg. Chem.* **35**, 527 (1987).
7. F. L. Carter, Ed., *Molecular Electronic Devices* (Dekker, New York, 1982); *Molecular Electronic Devices II* (Dekker, New York, 1987).
8. R. C. Haddon and A. A. Lamola, *Proc. Natl. Acad. Sci. U.S.A.* **82**, 1874 (1985).
9. J. S. Miller, *Adv. Mater.* **2**, 378 (1990); *ibid.*, p. 495; *ibid.*, p. 601.
10. J. Zarembowitch and O. Kahn, *New J. Chem.* **15**, 181 (1991).
11. S. Decurtins, P. Gütlich, C. P. Köhler, H. Spiering, A. Hauser, *Chem. Phys. Lett.* **105**, 1 (1984).
12. J. Zarembowitch *et al.*, *Mol. Cryst. Liq. Cryst.* **234**, 247 (1993).
13. C. Roux, J. Zarembowitch, B. Gallois, T. Granier, R. Claude, *Inorg. Chem.* **33**, 2273 (1994).
14. O. Kahn, J. Kröber, C. Jay, *Adv. Mater.* **4**, 718 (1992).
15. B. Gallois, J. A. Real, C. Hauw, J. Zarembowitch, *Inorg. Chem.* **20**, 1152 (1990).
16. J. A. Real, B. Gallois, T. Granier, F. Suez-Panamá, J. Zarembowitch, *ibid.* **31**, 4972 (1992).
17. T. Granier, B. Gallois, J. Gaultier, J. A. Real, J. Zarembowitch, *ibid.* **32**, 5305 (1993).
18. J. A. Real *et al.*, *J. Am. Chem. Soc.* **114**, 1979 (1992).
19. W. Vreugdenhil *et al.*, *Polyhedron* **9**, 2971 (1990).
20. At present, only a few examples of interpenetrating 2D networks are known. Some of them are shown in the following: J. Konnert and D. Britton, *Inorg. Chem.* **7**, 1193 (1966); R. W. Gable, B. F. Hoskins, R. Robson, *Chem. Commun.* **1990**, 1677 (1990); H. O. Stumpf, L. Ouahab, Y. Pei, D. Grandjean, O. Kahn, *Science* **261**, 447 (1993).
21. The compound $[Fe(tvp)_2(NCS)_2] \cdot CH_3OH$ was synthesized by slow addition of a methanolic solution (30 ml) containing an excess of tvp (6×10^{-3} mol) to a filtered methanolic solution (25 ml) prepared by mixing $Fe(ClO_4)_2 \cdot 6\,H_2O$ (10^{-3} mol) and KNCS (2×10^{-3} mol). The reaction was carried out under continuous stirring at 45°C. A deep red polycrystalline powder appeared in a few minutes. All operations were carried out under an argon atmosphere. The solid, stable in air, was washed with methanol and dried under vacuum.
22. The compound $[Fe(tvp)_2(NCS)_2] \cdot CH_3OH$ crystallizes in the tetragonal system, space group *P4/ncc* (number 130), with $a = b = 15.977(5)$ Å and $c = 15.368(4)$ Å (the number in parentheses is the error in the last digit), $V = 3922.9$ Å^3, $Z = 4$, $d_{calc} = 0.908$ g cm^{-3}, and λ (Mo Kα) = 0.71073 Å. The structure was solved by direct methods and successive Fourier difference syntheses. The refinements by full-matrix least-squares gave an *R* factor of 8.3 and a weighted *R* factor (R_w) of 6.5 from 860 reflections with intensity $I \geq 3\sigma(I)$ for 129 variables [weight = $9.5758/\sigma^2$ (*F*)]; linear absorption coefficient μ (Mo Kα) = 8.64 cm^{-1}. All nonhydrogen atoms were refined anisotropically. The methanol molecules are disordered; our recent x-ray single-crystal analysis on isostructural $[Co(tvp)_2(NCS)_2] \cdot CH_3OH$ confirms the number of solvent molecules per complex.
23. Sample A is obtained as a polycrystalline powder [see (*21*)]. Sample B consists of large single crystals obtained from slow diffusion (3 to 4 weeks) as mentioned above. Analytical data and x-ray powder diffraction of the different samples are the same, although significant differences can be observed in their magnetic curves.
24. G. Schill, *Catenanes, Rotaxanes, and Knots* (Academic Press, New York, 1971); D. M. Walba, *Tetrahedron* **41**, 3166 (1985); J. P. Sauvage, *Acc. Chem. Res.* **23**, 319 (1990); J. P. Sauvage *et al.*, *Chem. Rev.* **94**, 993 (1994).
25. V. Balzani and F. Scandola, *Supramolecular Photochemistry* (Horwood, Chichester, 1991).

26. We acknowledge financial assistance from the Dirección General de Investigación Científica y Técnica (DGICYT) (Spain) through Project PB91-0807-C02-01 and the Human Capital and Mobility Program (Network on Magnetic Molecular Materials from the EEC) through grant ERBCHRXCT920080. We are deeply indebted to J. Zarembowitch for her help in reviewing this contribution.

11 November 1994; accepted 10 February 1995

Imaging the Condensation and Evaporation of Molecularly Thin Films of Water with Nanometer Resolution

J. Hu,* X.-D. Xiao, D. F. Ogletree, M. Salmeron

The polarization force between an electrically charged atomic force microscope tip and a substrate has been used to follow the processes of condensation and evaporation of a monolayer of water on mica at room temperature. Condensation proceeds in two distinct structural phases. Up to about 25 percent humidity, the water film grows by forming two-dimensional clusters of less than a few 1000 angstroms in diameter. Above about 25 percent humidity, a second phase grows, forming large two-dimensional islands with geometrical shapes in epitaxial relation with the underlaying mica lattice. The growth of this second water phase is completed when the humidity reaches about 45 percent. The reverse process of evaporation has also been imaged.

The nanometer-scale structure of liquid films and surfaces is a fundamental subject of materials and biological sciences that has until now eluded a direct study because of the lack of suitable microscopy techniques with the required level of resolution. The growth of thin films of water is an important and largely unsolved problem in physics, chemistry, and biology. Water films alter the adhesion and lubricating properties of surfaces and the reactivity of solids with ambient gas molecules. The contact angle of water is used as a measure of the chemical activity of the surface. In biological processes, water films are critical for ion transport. Several studies have been recently devoted to the layering and orientation of water molecules on surfaces (*1–4*). Ice-like structures are predicted for the first layers, but no experimental evidence is available (*5–9*). Imaging water surfaces with nanometer resolution would make it possible to study many basic aspects of wetting, including condensation, evaporation, and chemical reactions. The validity of growth models and the structure of the first layers could be investigated at the molecular level.

Although modern scanning probe microscopes, like the scanning tunneling microscope (STM) and the atomic force microscope (AFM), have atomic-scale resolution, they cannot be easily used to study free liquid surfaces. For liquids, if the probe tip comes into contact with the surface, strong capillarity forces will cause the liquid to wet the tip and will strongly perturb the liquid. To avoid the bulging of the liquid surface that leads to wetting and capillary interaction, the tip must be kept at least several tens of angstroms from the imaging surface.

Our approach has been to use electrical polarization forces by applying a voltage to a conductive AFM tip with respect to a remote grounded electrode, for example, the sample holder (*10*). The strong electric field around the charged tip induces a polarization charge distribution on the surface of any nearby conductive or insulating materials. Because of the long-range nature of electrostatic interactions, the force can be detected at distances of several hundred of angstroms from the surface. This distance was determined by measuring the displacement of the

---

Materials Sciences Division, Lawrence Berkeley Laboratory, Berkeley, CA 94720, USA.

*Permanent address: Shanghai Institute of Nuclear Research, Academia Sinica, Post Office Box 800-204, Shanghai 201800, China.